PNAS RESEARCH ARTICLE | MEDICAL SCIENCES

Hereditary retinoblastoma iPSC model reveals aberrant spliceosome function driving bone malignancies

Jian Tu[a,b,c,1], Zijun Huo[a,d,1], Yao Yu[e], Dandan Zhu[a], An Xu[a], Mo-Fan Huang[a,f], Ruifeng Hu[g], Ruoyu Wang[f,h], Julian A. Gingold[i], Yi-Hung Chen[a], Kuang-Lei Tsai[f,h], Nicolas R. Forcioli-Conti[j], Sarah X. L. Huang[j], Thomas R. Webb[k], Jie Su[l], Danielle A. Bazer[m], Peilin Jia[g], Jason T. Yustein[n,o], Lisa L. Wang[p], Mien-Chie Hung[q,r,s], Zhongming Zhao[f,g], Chad D. Huff[e,f], Jingnan Shen[b,c], Ruiying Zhao[a,2], and Dung-Fang Lee[a,f,g,j,2]

Edited by Webster Cavenee, Ludwig Institute for Cancer Research Ltd., La Jolla, CA; received October 6, 2021; accepted March 9, 2022

The *RB1* gene is frequently mutated in human cancers but its role in tumorigenesis remains incompletely defined. Using an induced pluripotent stem cell (iPSC) model of hereditary retinoblastoma (RB), we report that the spliceosome is an up-regulated target responding to oncogenic stress in *RB1*-mutant cells. By investigating transcriptomes and genome occupancies in RB iPSC–derived osteoblasts (OBs), we discover that both E2F3a, which mediates spliceosomal gene expression, and pRB, which antagonizes E2F3a, coregulate more than one-third of spliceosomal genes by cobinding to their promoters or enhancers. Pharmacological inhibition of the spliceosome in *RB1*-mutant cells leads to global intron retention, decreased cell proliferation, and impaired tumorigenesis. Tumor specimen studies and genome-wide TCGA (The Cancer Genome Atlas) expression profile analyses support the clinical relevance of pRB and E2F3a in modulating spliceosomal gene expression in multiple cancer types including osteosarcoma (OS). High levels of pRB/E2F3a–regulated spliceosomal genes are associated with poor OS patient survival. Collectively, these findings reveal an undiscovered connection between pRB, E2F3a, the spliceosome, and tumorigenesis, pointing to the spliceosomal machinery as a potentially widespread therapeutic vulnerability of pRB-deficient cancers.

hereditary retinoblastoma | iPSCs | pRB | spliceosomal genes | osteosarcoma

Significance

Rare human hereditary disorders provide unequivocal evidence of the role of gene mutations in human disease pathogenesis and offer powerful insights into their influence on human disease development. Using a hereditary retinoblastoma (RB) patient–derived induced pluripotent stem cell (iPSC) platform, we elucidate the role of pRB/E2F3a in regulating spliceosomal gene expression. Pharmacological inhibition of the spliceosome in *RB1*-mutant cells preferentially increases splicing abnormalities of genes involved in cancer-promoting signaling and impairs cell proliferation and tumorigenesis. Expression of pRB/E2F3a–regulated spliceosomal proteins is negatively associated with pRB expression and correlates with poor clinical outcomes of osteosarcoma (OS) patients. Our findings strongly indicate that the spliceosome is an "Achilles' heel" of *RB1*-mutant OS.

The retinoblastoma gene family, also known as pocket proteins, includes three members, *RB1* (p105), *RBL1* (p107), and *RBL2* (p130) (1). In contrast to *RBL1* and *RBL2*, which are very rarely mutated in human cancers, *RB1* mutations are commonly found in various cancer types (2). Patients with hereditary retinoblastoma (RB), an inherited autosomal dominant cancer disorder caused by germline mutations/deletions in the *RB1* tumor suppressor gene, have a >400-fold increased incidence of osteosarcoma (OS) (3, 4), suggesting a strong mechanistic link between pRB loss and osteosarcomagenesis. By regulating E2F1/2/3 function, pRB fine-tunes the cell cycle (1) and cellular senescence (5). In addition to suppressing E2F transcriptional activities, pRB also modulates multiple cellular processes including apoptosis (6), centromeric and pericentromeric structure maintenance (7–9), homologous recombination (10), nonhomologous end joining (11), telomere preservation (12), and silencing of repetitive regions (13). These findings may contribute to some of the oncogenic phenotype associated with pRB loss, though the complete picture of pRB function in tumor suppression remains incompletely defined.

Alternative RNA splicing is a widespread biological process that allows for the expression of multiple RNA and protein isoforms from a single gene, contributing to structural transcript variation and proteome diversity in eukaryotes (14). Cancer cells exploit this process to express remarkable variation in transcriptome and splicing patterns (15, 16), often expressing unique cancer-specific splicing isoforms whose encoded proteins drive cancer progression or contribute to specific oncogenic features of the malignant cells. Expression levels of 261 known splicing factors were significantly more variable across 10 of 11 cancer types compared with normal noncancer controls (15). This altered variance supports the notion that dysregulation of spliceosomal genes is positively selected among cancers.

Several studies have revealed that pRB/E2F signaling regulates and is regulated by spliceosome function. A *Drosophila* study found that SR protein splicing factor B52 controls dE2F2 pre–messenger RNA (mRNA) splicing, suggesting that the spliceosome regulates pRB/E2F–mediated cell cycle control (17). Large-scale RNA interference screening in *Caenorhabditis elegans* revealed that partial inactivation of splicing-related genes overlaps with the pRB inactivation phenotype (18). Consistently, short hairpin RNA (shRNA) and CRISPR-Cas9 screening revealed that knockdown and/or knockout of RNA splicing factors induce lethal effects in pRB-deficient cancers (19, 20).

The authors declare no competing interest.

This article is a PNAS Direct Submission.

[1]J.T. and Z.H. contributed equally to this work.

[2]To whom correspondence may be addressed. Email: ruiying.zhao@uth.tmc.edu or dung-fang.lee@uth.tmc.edu.

This article contains supporting information online at http://www.pnas.org/lookup/suppl/doi:10.1073/pnas.2117857119/-/DCSupplemental.

Published April 11, 2022.

Investigation of pRB-interacting protein complexes also revealed that pRB physically interacts with RNA-binding proteins, implying that the pRB/E2F pathway may modulate RNA processes through posttranscriptional regulatory machinery (21). Although these studies imply the potential for regulation between pRB/E2F and spliceosome function, the involvement of pRB/E2F as a global regulator of spliceosomal gene expression, culminating in cancer development following pRB loss, has not been previously established.

In this study, we established RB induced pluripotent stem cells (iPSCs) and mutation-corrected isogenic control iPSCs and applied them to elucidate the pathological mechanisms of osteosarcomagenesis caused by *RB1* mutation. By integrating iPSC and cancer cell studies, we unexpectedly find that pRB loss leads to increased expression of numerous spliceosomal genes and that the spliceosome is a therapeutic vulnerability in *RB1*-mutant cancers.

Results

Generation, Characterization, and Mutation Correction of RB iPSCs. To elucidate how *RB1* mutation contributes to tumor initiation and progression, we generated iPSCs from fibroblasts obtained from members of a family including two affected RB patients (mother and daughter) and one unaffected individual (father) (Fig. 1*A*). The mother developed retinoblastoma and the daughter developed both retinoblastoma and OS. Whole-exome sequencing (WES) of these family members revealed that the two affected patients harbor a heterozygous c.1531-1532 ins A that causes a D511fs mutation, which was confirmed by Sanger sequencing (*SI Appendix*, Fig. S1 *A* and *B*). This D511fs mutation results in premature mRNA termination and decreased total pRB protein expression (*SI Appendix*, Fig. S1*C*). Using nonintegrating Sendai virus (SeV)–based cell reprogramming, we established iPSC clones from the affected and unaffected family members. These iPSC clones demonstrated human embryonic stem cell (hESC) morphology and expressed pluripotency factors (NANOG and OCT4), hESC surface markers (TRA-1-81 and SSEA4), and alkaline phosphatase (AP) (Fig. 1*B*). The lines also showed expression of pluripotency markers at levels comparable to H1 and H9 hESCs by qRT-PCR (*SI Appendix*, Fig. S1*D*). Consistent with their genotype, RB iPSCs demonstrated lower pRB protein than wild-type (WT) iPSCs (*SI Appendix*, Fig. S1*E*). We further verified the loss of SeV and exogenous *OCT4*, *SOX2*, *KLF4*, and *MYC* transgenes (*SI Appendix*, Fig. S1*F*), demonstrating that these WT and RB iPSCs have zero genetic footprints from reprogramming. Both WT and RB iPSC lines were karyotypically normal (*SI Appendix*, Fig. S1*G*) and demonstrated the capacity to differentiate into all three germ layers in teratomas (*SI Appendix*, Fig. S1*H*). Together, our results indicate that somatic cells from RB patients can be properly reprogrammed, maintain a pluripotent state, and be effectively differentiated. The characteristics of WT and RB iPSCs are summarized in *SI Appendix*, Table S1.

In order to generate isogenic controls and correct *RB1* mutation in RB iPSCs, we applied CRISPR-Cas9 nickase constructs targeting the *RB1* genome locus. The CRISPR-Cas9 nickase system minimizes off-target mutations by 50- to 1,500-fold compared with a CRISPR system inducing double-stranded breaks in cultured cells (22). The paired nickase plasmids were designed to target *RB1* intron 16 (c.1531-1532 ins A located in *RB1* exon 17) (Fig. 1*C*). The T7E1 assay validated on-target CRISPR-Cas9 editing events following treatment with CRISPR-Cas9 nickase plus single-guide RNA (sgRNA) pairs (*SI Appendix*, Fig. S1*I*). The CRISPR-Cas9 plasmids and donor vector containing an FNF/Neo^R selection cassette (Frt-EM7-Neo^R-Frt) with 1-kb homologous arms were constructed and electroporated into RB iPSCs and selected with G418. Resistant clones were examined for FNF insertion in intron 16 of the *RB1* genomic locus by PCR (*SI Appendix*, Fig. S1*J*). Southern blot analysis confirmed the unique FNF insertion in the *RB1* genomic locus (*SI Appendix*, Fig. S1*K*). Once the corrected clones were confirmed by Sanger sequencing, we excised the FNF/Neo^R cassette by Flp recombinase (*SI Appendix*, Fig. S1*L*). Mutation-corrected iPSC lines (corrected RB [cRB] iPSCs) demonstrated a corrected *RB1* gene sequence (Fig. 1*D*) and expression of the restored pRB protein (Fig. 1*E*). The efficiency of correcting the *RB1* gene mutation with this CRISPR-Cas9 nickase system was 0.5 to 2.3% (*SI Appendix*, Fig. S1*M*).

RB iPSC-Derived Osteoblasts Demonstrate a Premalignant Phenotype. RB patients are susceptible to developing second cancers such as sarcomas, melanomas, and brain cancers. Among them, OS is the leading cause of death in RB survivors (3, 4). One RB patient in our studied family had already developed OS (Fig. 1*A*). The *RB1* gene is also frequently mutated in OS from patients without *RB1* germline mutations (4). We applied the RB iPSC model to understand the pathogenesis of OS caused by *RB1* mutation. Prior studies have suggested that OS likely arises from the acquisition of malignant features within osteoblasts (OBs) (4, 23). Since human OBs can be induced from multipotent mesenchymal stem cells (MSCs), our iPSC model could be used to assess the effects of *RB1* mutation in OBs. We first differentiated WT, RB, and cRB iPSCs to their corresponding MSCs. These iPSC-derived MSCs expressed the MSC surface markers CD105 and CD166 but not pluripotent marker CD24 (*SI Appendix*, Fig. S2*A*). In comparison with cRB MSCs, RB MSCs showed higher mRNA expression of numerous pRB/E2F targets *CCNA2*, *CDC6*, *CDK1*, *BRCA1*, and *RAD51* (*SI Appendix*, Fig. S2*B*) and E2F transcriptional reporter activity (*SI Appendix*, Fig. S2*C*). These studies demonstrate that RB MSCs maintain comparable cell-surface marker expression to WT and cRB MSCs and that RB MSCs partially lack pRB function while mutation-corrected cRB cells have restored pRB function.

MSCs were then induced to OBs as the osteogenic differentiation process was monitored over time (23–25). Consistent with mouse studies showing enhanced osteogenic differentiation upon loss of pRb (26), RB OBs showed increased bone-associated AP activity at day 6 (*SI Appendix*, Fig. S2*D*), mineral deposition at days 15 and 24 (*SI Appendix*, Fig. S2*E*), and expression of skeletal system development genes *ANKH*, *CLEC3B*, and *IGF2* at day 24 (*SI Appendix*, Fig. S2*F*). We compared expression levels of core transcriptional/epigenetic regulators in RB and cRB cells during osteogenic differentiation. None of the core osteogenic regulators, including ATF4, CEBPD, RUNX2, ZEB1, and ZNF521, showed impaired expression during osteogenic differentiation (*SI Appendix*, Fig. S2*G*), indicating that loss of pRB has a limited impact on the osteoblastic transcription factor network. To investigate whether RB OBs are able to recapitulate tumorigenic potential, we performed in vitro anchorage-independent growth (AIG) assays and in vivo xenografts. AIG assays showed clonal growth in soft agar by RB OBs but not WT and cRB OBs (Fig. 1*F*). In vivo xenograft assays demonstrated in vivo cell proliferation abilities in RB OBs but not WT and cRB OBs (Fig. 1*G*). The characteristics of WT, RB, and cRB iPSC-derived MSCs and OBs are summarized in *SI*

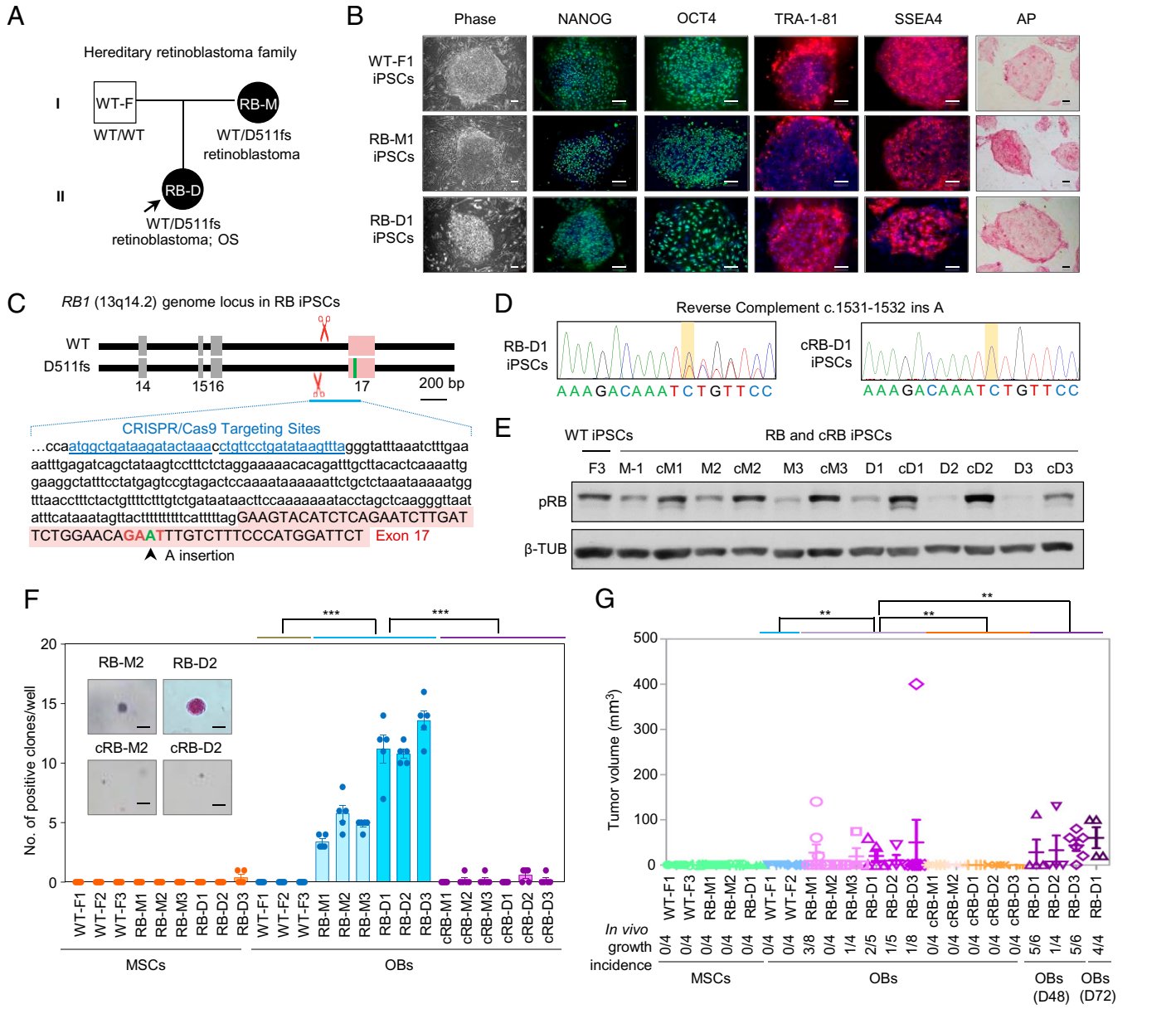

Fig. 1. Generation of a premalignant RB patient–derived iPSC platform. (*A*) The RB family tree includes two RB patients (mother: RB-M; daughter: RB-D) with a heterozygous pRB(D511fs) mutation and one unaffected relative (father: WT-F). Arrow, proband. (*B*) SeV-4F (OCT4, SOX2, KLF4, and MYC)–reprogrammed RB and WT iPSCs highly express hESC pluripotency factors (NANOG and OCT4) and hESC surface markers (TRA-1-81 and SSEA4) and have high AP activity. (Scale bars, 100 μm.) (*C*) Schematic overview of correcting *RB1* mutation by CRISPR-Cas9 nickase in the *RB1* genomic locus (13q14.2). CRISPR-Cas9 sgRNA target sites are labeled in blue. *RB1* exon 17 is labeled in pink. The c.1531-1532 ins A site is labeled in green and the affected GAT nucleotide encoding aspartic acid (D) is colored red. (*D*) Sanger sequencing indicates the *RB1* c.1531-1532 ins A mutation is corrected in cRB iPSCs. (*E*) Western blot reveals comparable pRB protein levels in WT and cRB iPSCs and lower levels in RB iPSCs, indicating restoration of pRB protein upon correction of *RB1* gene mutation. (*F*) AIG assay demonstrates in vitro tumorigenic ability for RB OBs but not WT and cRB OBs. Colonies larger than 50 μm after 1 mo of growth are considered positive. (Scale bars, 100 μm.) Representative photographs show positive colonies from RB-M2 and RB-D2 OBs. (*G*) Tumor xenograft experiments by subcutaneous transplantation in *NU/NU* mice demonstrate that RB but not WT or cRB OBs recapture in vivo cell proliferation ability. The numbers of xenografts are indicated. Results are expressed as mean ± SEM. **P* < 0.05, ***P* < 0.01, ****P* < 0.001.

Appendix, Table S1. In summary, our findings demonstrated a premalignant phenotype for RB iPSC-derived OBs.

RB OBs Demonstrate an Up-Regulated RNA Spliceosomal Gene Signature. In order to gain insights into pRB loss–induced oncogenic effects, we investigated and compared global transcripts among WT, RB, and cRB OBs. mRNAs were isolated at three differentiation time points (day 0, MSCs; day 15, pre-OBs; day 24, OBs) and analyzed by RNA sequencing (RNA-seq). Spearman's correlation demonstrated that gene expression profiles from MSCs are distinct from pre-OB and OB samples (Fig. 2*A*), suggesting successful osteogenic differentiation in WT, RB, and cRB cells. As expected, levels of numerous known pRB/E2F targets were up-regulated in RB OBs compared with both WT and cRB OBs (*SI Appendix*, Fig. S3*A*). Gene set enrichment analysis (GSEA) of transcription factor targets and oncogenic signatures identified E2F chromatin immunoprecipitation (ChIP) targets and a pRB/E2F–associated oncogenic signature as enriched in RB OBs (*SI Appendix*, Fig. S3 *B* and *C*). Consistent with loss of pRB facilitating osteogenic differentiation (*SI Appendix*, Fig. S2 *D*–*F*), genes up-regulated in RB OBs compared with WT and cRB OBs at day 24 were most highly

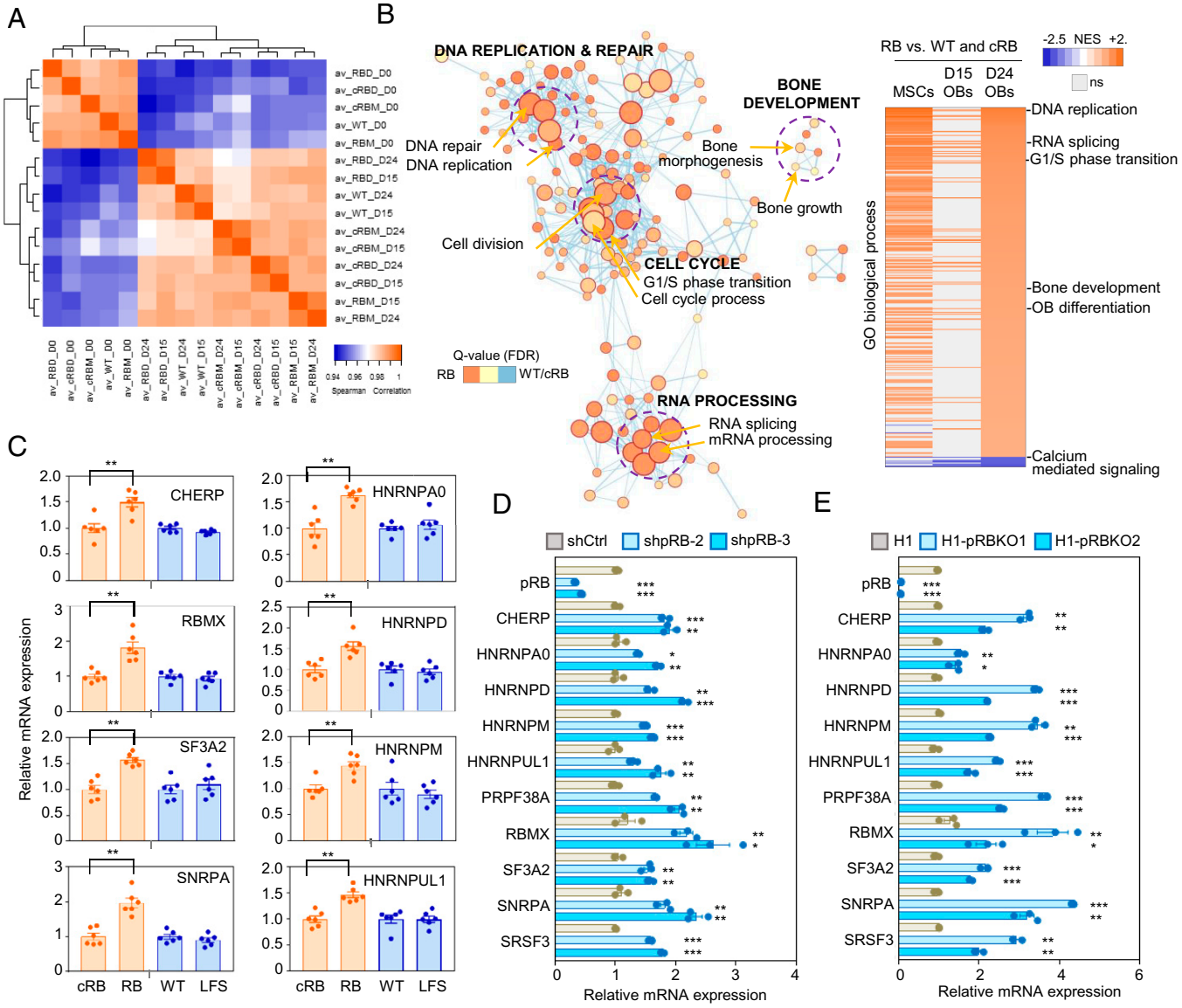

Fig. 2. Enrichment of RNA splicing and spliceosomal genes in RB iPSC-derived OBs. (*A*) Heatmap demonstrating a pairwise comparison of gene expression levels from WT, RB, and cRB RNA-seq during the time course of differentiation by Spearman's correlation. The pairwise correlation coefficients range from 0.94 (blue) to 1 (orange). (*B*, *Left*) Enrichment of GO biological processes identified by EnrichmentMap analysis. Network visualization of enriched gene sets in RB OBs compared with WT and cRB OBs at day 24 indicates that GO biological processes involved in DNA replication and repair, cell cycle, RNA process, and bone development are enriched in RB OBs. Enriched gene sets in RB OBs are displayed in orange and enriched gene sets in WT and cRB OBs are shown in blue. FDR, false discovery rate. (*B*, *Right*) Enriched GO biological processes in RB vs. WT and cRB OBs are analyzed by GSEA and summarized by a heatmap. Nonsignificant GOs are shown in light gray. (*C*) qRT-PCR indicates that expression of spliceosomal genes is enriched in RB iPSC-derived OBs but not LFS iPSC-derived OBs compared with their corresponding WT controls. (*D*) qRT-PCR demonstrates that depletion of pRB in WT OBs leads to up-regulation of spliceosomal genes. (*E*) qRT-PCR indicates that H1-pRBKO hESC-derived OBs demonstrate increased spliceosomal gene expression compared with H1 hESC-derived OBs. Results are expressed as mean ± SEM. $*P < 0.05$, $**P < 0.01$, $***P < 0.001$.

expressed in more terminally differentiated (day 21) mouse OB gene profiles as well as in an RB gene-associated cancer signature (*SI Appendix*, Fig. S3*D*).

Genomic alterations and rearrangements are commonly found in human OS (27, 28). To investigate if RB iPSC-derived OBs also harbor these rearrangements, we applied in silico cytogenetic region enrichment analysis (CREA) (23) to RB OB samples to identify the potential presence of rearranged regions frequently found in human OS. CREA revealed that chromosomal rearrangements are uncommon in these RB iPSC-derived OBs (*SI Appendix*, Fig. S3*E*), suggesting that RB iPSC-derived OBs can model the early stages of OS initiation and progression caused solely by *RB1* mutation prior to the acquisition of secondary genomic alterations. Furthermore, GSEA demonstrated that differentially expressed genes in OS compared with normal OBs are specifically enriched in RB OBs compared with WT and cRB OBs at day 24 (*SI Appendix*, Fig. S3*F*), indicating that RB OBs nonetheless acquire genes associated with an OS signature in the absence of additional gene alterations.

Gene ontology (GO) analyses revealed that RB OBs are enriched for genes involved in DNA replication and repair, cell cycle (e.g., cell cycle process and G1/S phase transition), RNA processing (e.g., RNA splicing and mRNA processing), and bone development (e.g., bone morphogenesis, bone growth, and OB differentiation) (Fig. 2*B*). Surprisingly, the enrichment of RNA processing pathways was not clearly noted in previous studies. qRT-PCR verified that numerous spliceosomal genes (e.g., *CHERP*, *HNRNPA0*, *HNRNPD*, *HNRNPM*, *HNRNPUL1*, *SF3A2*, *SNRPA*, and *RBMX*) are enriched in RB OBs (Fig. 2*C*).

The enrichment of spliceosomal genes is unique to RB but not Li–Fraumeni syndrome (LFS) OBs, despite the fact that the hereditary cancer syndrome LFS also carries an OS predisposition, indicating a pRB-specific effect. shRNA-mediated pRB knockdown in WT iPSC-derived OBs led to increased expression of numerous spliceosomal genes (Fig. 2*D*). To verify if the regulation of spliceosomal genes by pRB is a common phenomenon, we generated pRB-knockout (pRBKO) hESC H1 lines by CRISPR-Cas9 and differentiated these cells to OBs (*SI Appendix*, Fig. S3*G*). Compared with H1-derived OBs, H1-pRBKO–derived OBs consistently expressed elevated spliceosomal genes (Fig. 2*E*). In contrast, overexpression of pRB resulted in the down-regulation of spliceosomal gene expression in RB OBs (*SI Appendix*, Fig. S3*H*). In comparison with normal retinal tissues, GSEA of retinoblastoma revealed enrichment of GO biological process RNA splicing and Kyoto Encyclopedia of Genes and Genomes (KEGG) spliceosome (*SI Appendix*, Fig. S3*I*). In summary, these findings demonstrate that pRB negatively regulates spliceosomal gene expression across multiple OB and OS lines and tissues and emphasize that spliceosomal dysregulation is involved in pRB loss–induced oncogenesis.

pRB Selectively Binds to E2F3a-Targeted Spliceosomal Genes. pRB functions as a transcriptional corepressor and many of its tumor-suppression functions have been attributed to its ability to negatively regulate E2F-mediated cell cycle gene programs. Among pRB-interacting E2F family members, E2F3a, but not E2F1 and E2F2, is predominantly expressed in OBs (*SI Appendix*, Fig. S4*A*). We hypothesized that pRB binds to E2F3a and negatively modulates E2F3a-regulated spliceosomal gene expression. To address this hypothesis, we carried out pRB and E2F3a chromatin immunoprecipitation followed by next-generation sequencing (ChIP-seq) to determine whether the selective up-regulation of spliceosomal genes in RB OBs is due to preferential binding of pRB and E2F3a to the promoters of these genes. ChIP-seq analyses revealed a striking degree of genome-wide overlap between pRB and E2F3a sites (Fig. 3*A*). More than one-third of pRB-only (2,889), pRB/E2F3a–cotargeted (4,096), and E2F3a-only (6,539) peaks were detected at promoters and transcription start sites (TSSs) (*SI Appendix*, Fig. S4*B*), indicating preferential binding of pRB and E2F3a to gene-proximal regions of transcription initiation. De novo motif analyses revealed that the top motif enriched in pRB/E2F3a–co-occupied sites is identical to the E2F family motif (*SI Appendix*, Fig. S4*C*). In addition, pRB ChIP-seq read densities of pRB/E2F3a–co-occupied peaks were significantly higher than those of pRB-only peaks, suggesting that the localization of pRB to chromatin is dependent on E2F3a (*SI Appendix*, Fig. S4*D*).

To determine specific functional categories modulated by pRB and E2F3a simultaneously, we performed functional enrichment analysis on the enriched genomic regions co-occupied by pRB and E2F3a. pRB/E2F3a–cotargeted genes were highly enriched for ontologies of processing of capped introns containing pre-mRNA, mRNA splicing, and RNA processing (Fig. 3*B*). These cotargeted gene ontologies were even better enriched than well-known pRB- and E2F-modulated ontologies such as the cell cycle and telomere maintenance (Fig. 3*B*). We then analyzed the promoter/TSS regions of 134 critical spliceosomal proteins for potential pRB and E2F3a binding. More than one-third (50 of 134) of spliceosomal gene promoter/TSS regions were cobound by both pRB and E2F3a (Fig. 3 *C*, *Upper*), and expression of these spliceosomal genes was increased in RB OBs compared with cRB OBs (Fig. 3 *C*, *Lower*). These findings confirm the critical function of pRB and E2F3a in regulating global spliceosomal gene expression.

The spliceosomal genes cobound by pRB and E2F3a at the promoter/TSS regions by ChIP-seq included *CHERP*, *HNRNPA0*, *HNRNPD*, *HNRNPM*, *HNRNPUL1*, *PRPF38A*, *SF3A2*, and *SNRPA* (Fig. 3*D* and *SI Appendix*, Fig. S4*E*). ChIP-qPCR validated the binding of pRB and E2F3a to *HNRNPD*, *HNRNPUL1*, *SF3A2*, and *SNRPA* promoter regions but not to regions adjacent to and upstream of the peak regions (Fig. 3*E*). pRB and E2F3a ChIP specificities were further verified by exogenous Flag-tagged pRB and E2F3a ChIP-qPCR (*SI Appendix*, Fig. S4*F*). Furthermore, E2F3a increased the expression of these spliceosomal genes (*SI Appendix*, Fig. S4*G*), supporting our hypothesis that pRB negatively regulates spliceosomal gene expression by inhibiting E2F3a. Taken together, these ChIP-seq studies provide a direct mechanistic link between pRB/E2F3a transcriptional regulatory machinery and global spliceosomal gene expression.

pRB and E2F3a Coregulate Distal Enhancers of Spliceosomal Genes. The analysis of the genomic distribution of pRB/E2F3a–cotargeted binding sites demonstrated that more than half of RB1/E2F3a–cotargeted peaks were not located at promoter or TSS regions (*SI Appendix*, Fig. S4*B*). For example, RBMX was up-regulated in pRB-deficient cells, but ChIP-seq analysis showed that both pRB and E2F3a barely bind the *RBMX* promoter and TSS regions, suggesting that other regulatory mechanisms (e.g., enhancers) are involved in pRB/E2F3a–regulated *RBMX* gene expression. We found that 31.0% of pRB- and 32.7% of E2F3a-occupied peaks are marked by H3K27ac (a putative enhancer marker) in OBs and multiple OS lines (*SI Appendix*, Fig. S5*A*). These findings support a regulatory role for pRB and E2F3a on distal enhancers. Indeed, pRB and E2F3a co-occupy putative enhancer regions of some spliceosomal genes including *RBMX* (*SI Appendix*, Fig. S5*B*). ChIP-qPCR validated the binding of pRB and E2F3a to *RBMX* enhancer regions but not upstream of the peak regions (*SI Appendix*, Fig. S5*C*). To demonstrate that these putative pRB/E2F3a–bound distal elements represent bona fide enhancers for *RBMX*, we performed CRISPR-Cas9–mediated deletion on this upstream region of *RBMX*. Two sgRNAs were designed to target upstream and downstream of the putative *RBMX* enhancer regions, thus creating a 676-bp deletion (*SI Appendix*, Fig. S5*D*). Sanger sequencing of sgRNA-transduced RB OBs demonstrated that CRISPR-Cas9–mediated on-target editing leads to a 676-bp deletion in the targeted pRB/E2F3a–cobound peak region (*SI Appendix*, Fig. S5*E*). Deletion of this *RBMX* upstream region indeed reduced expression of *RBMX* (*SI Appendix*, Fig. S5*F*), suggesting its function as a distal enhancer. Furthermore, the epigenomic perturbation of the *RBMX* upstream region by CRISPR interference (CRISPRi)–targeted inhibition (29) and CRISPR activation (CRISPRa)–targeted activation (30) demonstrated that CRISPRi suppresses *RBMX* expression (*SI Appendix*, Fig. S5*G*) while CRISPRa increases *RBMX* expression (*SI Appendix*, Fig. S5*H*). These findings demonstrate that pRB and E2F3a can modulate spliceosomal gene expression through distal regulatory elements. Collectively, our results emphasize that pRB and E2F3a coordinate the expression of spliceosomal genes across multiple transcriptional regulatory layers.

Spliceosome Perturbation in RB OBs Selectively Increases Retained Intron Events and Hampers Cell Proliferation. To further assess the effect of the spliceosomal perturbation on global splicing patterns between RB and cRB OBs, we

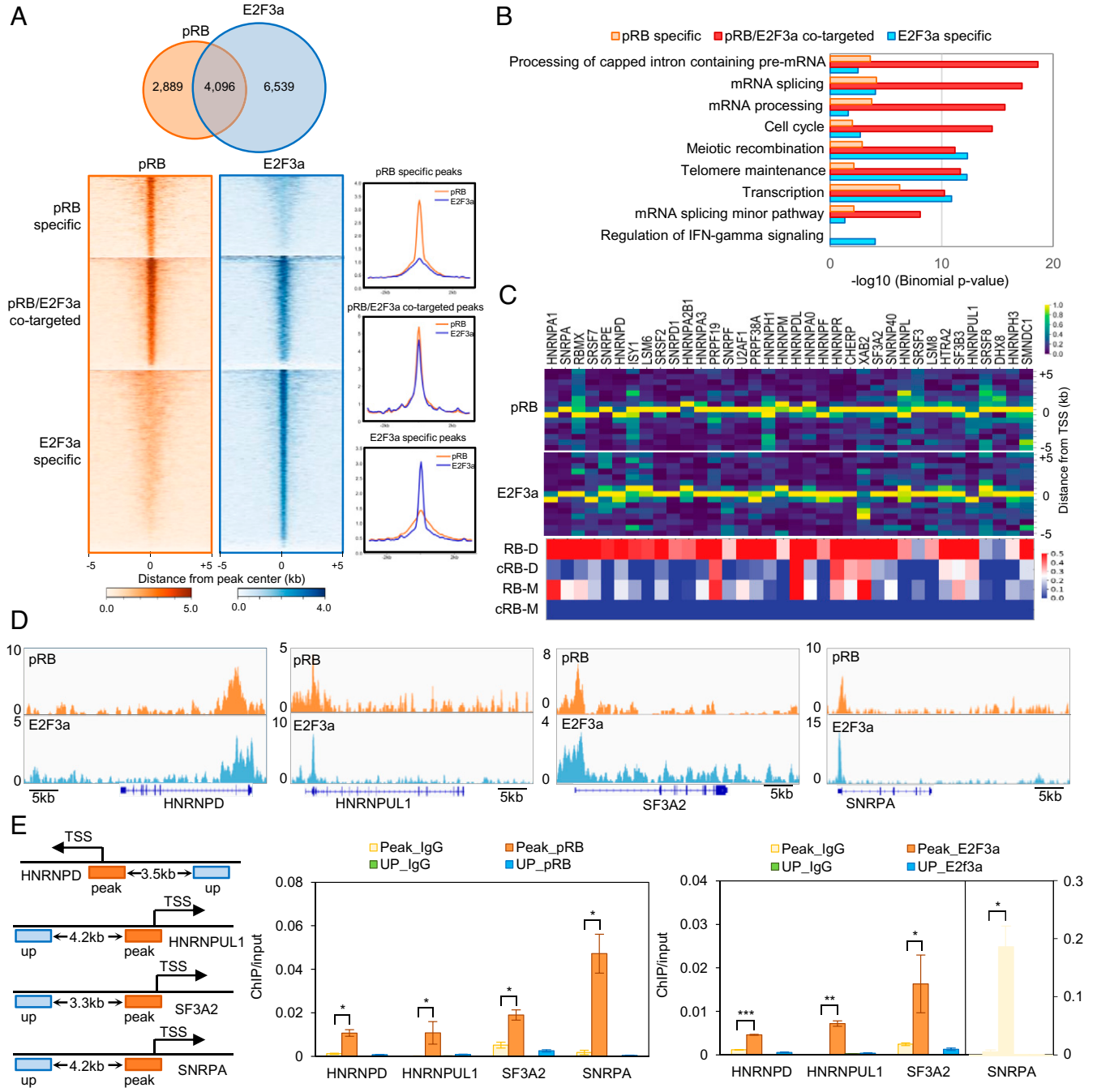

Fig. 3. pRB and E2F3a directly cotarget spliceosomal genes. (*A*, *Top*) Venn diagram depicts the overlap between pRB and E2F3a binding peaks in cRB OBs and defines pRB-specific (2,889), pRB/E2F3a–cotargeted (4,096), and E2F3a-specific (6,539) loci. (*A*, *Bottom Left*) Heatmaps depict pRB and E2F3a binding to the 5-kb genomic loci surrounding the identified ChIP-seq peaks, grouped by cluster. (*A*, *Bottom Right*) Composite plots show the average binding of pRB and E2F3a to the pRB-specific, pRB/E2F3a–cotargeted, and E2F3a-specific loci. (*B*) GO analyses of pRB-specific, pRB/E2F3a–cotargeted, and E2F3a-specific genomic regions. pRB/E2F3a–cotargeted genes are overrepresented for numerous RNA splicing pathway genes, including those involved in the processing of capped introns containing pre-mRNA, mRNA splicing, mRNA processing, and mRNA splicing minor pathway. (*C*) Increased expression of pRB/E2F3a–cotargeted spliceosomal genes in RB OBs compared with cRB OBs. (*C*, *Upper*) Heatmaps of ChIP-seq peak intensities in pRB/E2F3a–cotargeted spliceosomal gene regions (±5 kb from the TSS). Each box in the heatmap represents a 0.7-kb region. (*C*, *Lower*) Heatmap of spliceosomal gene expression in RB-D, RB-M, cRB-D, and cRB-M OBs is examined by RNA-seq. (*D*) Integrative Genomics Viewer snapshot of pRB and E2F3a occupancy over promoter regions of spliceosomal genes *HNRNPD*, *HNRNPUL1*, *SF3A2*, and *SNRPA*. (*E*) ChIP-qPCR validation of pRB and E2F3a binding peaks at identified spliceosomal genes. (*E*, *Left*) Schematic of amplicon locations of spliceosomal genes and upstream controls used for ChIP-qPCR validation. (*E*, *Right*) ChIP-qPCR at spliceosomal TSS peak sites and upstream controls to assess for pRB (*Left*), E2F3a (*Right*), or immunoglobulin G (IgG) enrichment (ChIP/input). ChIP-qPCR confirms specific enrichment of *HNRNPD*, *HNRNPUL1*, *SF3A2*, and *SNRPA* at peak regions in RB OBs. Results are expressed as mean ± SEM. **P* < 0.05, ***P* < 0.01, ****P* < 0.001.

performed pairwise percent spliced-in (PSI) analyses of exons among spliceosome inhibitor pladienolide B (PB)–treated cells. Different splicing events, including alternative 5′ splicing site (A5), alternative 3′ splicing site (A3), alternative first exon (AF), alternative last exon (AL), mutually exclusive exon (MX), retained intron (RI), and skipped exon (SE), were examined. Despite global increases in pRB/E2F3a–mediated gene transcription events in RB OBs, PSI analyses identified no obvious frequency differences in splicing events between RB and cRB OBs (Fig. 4*A*), implying that the up-regulation of spliceosomal genes following pRB depletion overcomes up-regulated RNA transcription and prevents splicing defects. In contrast,

spliceosomal inhibition by PB increased RI events in RB OBs compared with cRB OBs (Fig. 4 *A* and *B*). Interestingly, aberrant RIs were the primary alternative splicing event that increased following inhibition of spliceosomal function by PB in RB OBs compared with cRB OBs, while other alternative splicing events remained comparable (Fig. 4*B*). RNA-seq demonstrated that PB treatment increased aberrant RIs in tumor-associated genes *METTL2B*, *JAG1*, *ZC3HAV1*, and *BYSL* in RB OBs compared with cRB OBs (Fig. 4*C*). PCR confirmed the increase of RIs on intron 1 in METTL2B mRNA, intron 12 in *JAG1* mRNA, intron 3 in *ZC3HAV1* mRNA, and intron 6 in *BYSL* mRNA (Fig. 4*C*). Neither treatment with PB nor presence of *RB1* mutation in OBs was associated with any significant difference in the intron length of transcripts containing RIs or SEs (*SI Appendix*, Fig. S6*A*). PB-induced RI and SE events were broadly observed in all transcripts and independent of transcript lengths (*SI Appendix*, Fig. S6*B*). STREME (sensitive, thorough, rapid, enriched motif elicitation)-enriched motif analysis of the 50-bp intronic sequence from each end of an RI event in PB-treated RB and cRB OBs demonstrated an enriched ACTYAC motif in RI-affected transcripts upon PB treatment (*SI Appendix*, Fig. S6*C*). Suppression of spliceosomal function by PB preferentially enhanced splicing events in pRB and pRB/E2F3a targets (Fig. 4*D*). Transcripts with RIs that were pRB/E2F3a targets were more highly expressed than global transcripts (with or without RIs) (Fig. 4*E*). Together, these results suggest that pRB and pRB/E2F3a targets are relatively vulnerable to spliceosome inhibition.

Interestingly, the transcripts with lower RIs in RB OBs had a significant increase in RIs upon spliceosome inhibition (*SI Appendix*, Fig. S6*D*), indicating that an increase in pRB/E2F3a onco-spliceosome signature (REOSS) gene expression in *RB1*-mutant OBs prevented RI events from occurring in certain transcripts, but that these transcripts showed impaired splicing and increased RIs upon spliceosome inhibition. Examination of 47 previously identified cancer-related alternatively spliced isoforms (15, 16) including MCL1, MDM2, and CD44 revealed that only MDM2 AF decreased in PB-treated RB OBs compared with PB-treated cRB OBs (*SI Appendix*, Fig. S6*E*). Notably, MDM2 alternative splicing isoforms were suggested to convey p53-dependent and independent tumor-promoting abilities (31). Pathway analysis of genes with perturbed splicing events revealed that gene transcripts involved in OS-associated signaling pathways, such NOTCH, TGFβ, α5β3-integrin, and NF-κB, were markedly more likely to have RIs in RB OBs compared with cRB OBs upon PB treatment (Fig. 4*F*). These results suggest that inhibition of spliceosomal function preferentially impairs RIs and OS-associated oncogenic gene functions in RB OBs. We further examined if pharmacological inhibition of the spliceosome also impaired the cell proliferation potential of RB OBs. Compared with cRB OBs, RB OBs were significantly more sensitive to spliceosome inhibitors SD6 (32) and PB (Fig. 4 *G* and *H*). These findings imply that, in contrast to cRB OBs, premalignant RB OBs confer hyperdependency on spliceosome function for proliferation and survival.

pRB-Deficient OS Lines Are Sensitive to Spliceosome Perturbation. Since up-regulation of spliceosomal genes in pRB-deficient cells may overcome the final bottleneck to osteosarcomagenesis, we thus investigated whether the spliceosome is an exploitable vulnerability in pRB-deficient cancers. We labeled the 51 spliceosomal genes coregulated by pRB and E2F3a as the REOSS. Knockdown of REOSS genes (*HNRNPUL1*, *RBMX*, *SF3A2*, and *SNRPA*) but not non-REOSS genes (*BUD31*, *SRSF9*, *U2AF2*, and *XAB2*) selectively reduced cell numbers in HOS-pRBKO cells compared with HOS-Ctrl (control) cells (Fig. 5 *A* and *B*). Ectopic expression of REOSS genes (*HNRNPUL1*, *RBMX*, *SF3A2*, and *SNRPA*) promoted cell proliferation and increased colony-forming activity in HOS cells (Fig. 5 *C* and *D*). These findings indicate that up-regulation of REOSS genes, at least *HNRNPUL1*, *RBMX*, *SF3A2*, and *SNRPA*, plays a role in promoting tumor growth in pRB-deficient OS. Cell viability assay and fluorescence-based competition assay indicated that both SD6 and PB selectively suppress HOS-pRBKO cells compared with HOS-Ctrl cells (Fig. 5*E* and *SI Appendix*, Fig. S7*A*). Consistently, the colony-forming assay demonstrated sensitivity of pRBKO and pRB-knockdown 143B cells to PB-mediated inhibition (*SI Appendix*, Fig. S7 *B* and *C*). Stable transfection of pRB in Saos2 cells led to resistance to spliceosome inhibitors (*SI Appendix*, Fig. S7*D*). Treatment of OS xenografts from the 143B OS line with SD6 potently restrained in vivo tumorigenesis in 143B-pRBKO cells but less so in 143B-Ctrl cells, emphasizing that the spliceosome is essential for tumorigenicity of pRB-deficient OS (Fig. 5*F*).

To determine the clinical relevance of the pRB/E2F3a–regulated REOSS in osteosarcomagenesis, we examined the expression of selected REOSS genes (SNRPA, CHERP, HNRNPD, and RBMX) across 74 human OS specimens by immunohistochemical (IHC) staining. CHERP was detected in 15 (38.5%) of 39 specimens with low pRB expression but in only 6 (17.1%) of 35 specimens with high pRB expression, indicating that CHERP expression is associated with low levels of pRB ($P < 0.05$; Fig. 5*G*). In contrast, CHERP was detected in 18 (36%) of 50 specimens with high E2F3a expression but in only 3 (12.5%) of 24 specimens with low E2F3a expression, suggesting that CHERP expression is associated with high levels of E2F3a ($P < 0.05$; Fig. 5*H*). Similarly, HNRNPD, SNRPA, and RBMX were also negatively associated with pRB expression (HNRNPD, $P < 0.05$; SNRPA, $P = 0.058$; RBMX, $P < 0.05$; Fig. 5*G*) but strongly associated with E2F3a expression (HNRNPD, $P < 0.05$; SNRPA, $P < 0.001$; RBMX, $P < 0.001$; Fig. 5*H*). We next analyzed the expression of these REOSS genes in OS tumor tissues and correlated them with reported patient survival data. The Kaplan–Meier overall survival curves showed that low pRB and high E2F3a, CHERP, HNRNPD, SNRPA, and RBMX levels are associated with poor survival (*SI Appendix*, Fig. S7 *E–J*). Taken together, OS IHC studies suggest that pRB/E2F3a–regulated spliceosomal genes contribute to osteosarcomagenesis and are associated with poor clinical outcomes in OS patients.

pRB/E2F3a Regulate REOSS Gene Expression in Multiple Cancer Types with High *RB1* Mutation Rates. To determine whether our findings can be generalized to other cancers, we next explored pRB/E2F3a regulation of REOSS gene features in other human cancers by analyzing the expression of REOSS genes across 34 human cancers in The Cancer Genome Atlas (TCGA) pan-cancer datasets. TCGA pan-cancer transcriptome data revealed that expression of a group of REOSS genes is significantly elevated in pRB-low cancers (e.g., TGCT, UVM, DLBC, BRCA, UCS, GBM, LUAD, LUSC, SARC, ACC, OV, BLCA, ESCA, UCEC, CHOL, THCA, PAAD, LIHC, CESC, and HNSC) (*SI Appendix*, Fig. S8*A*) and E2F3-high cancers (e.g., SKCM, UVM, THYM, UCEC, GBM, TGCT, BRCA, COAD, LUSC, OV, LGG, LIHC, READ, STAD, LUAD, LUNG, BLCA, ESCA, PRAD, SARC, CESC, and HNSC) (*SI Appendix*, Fig. S8*B*). These pRB/E2F3a–regulated cancers included multiple cancer types characterized by high

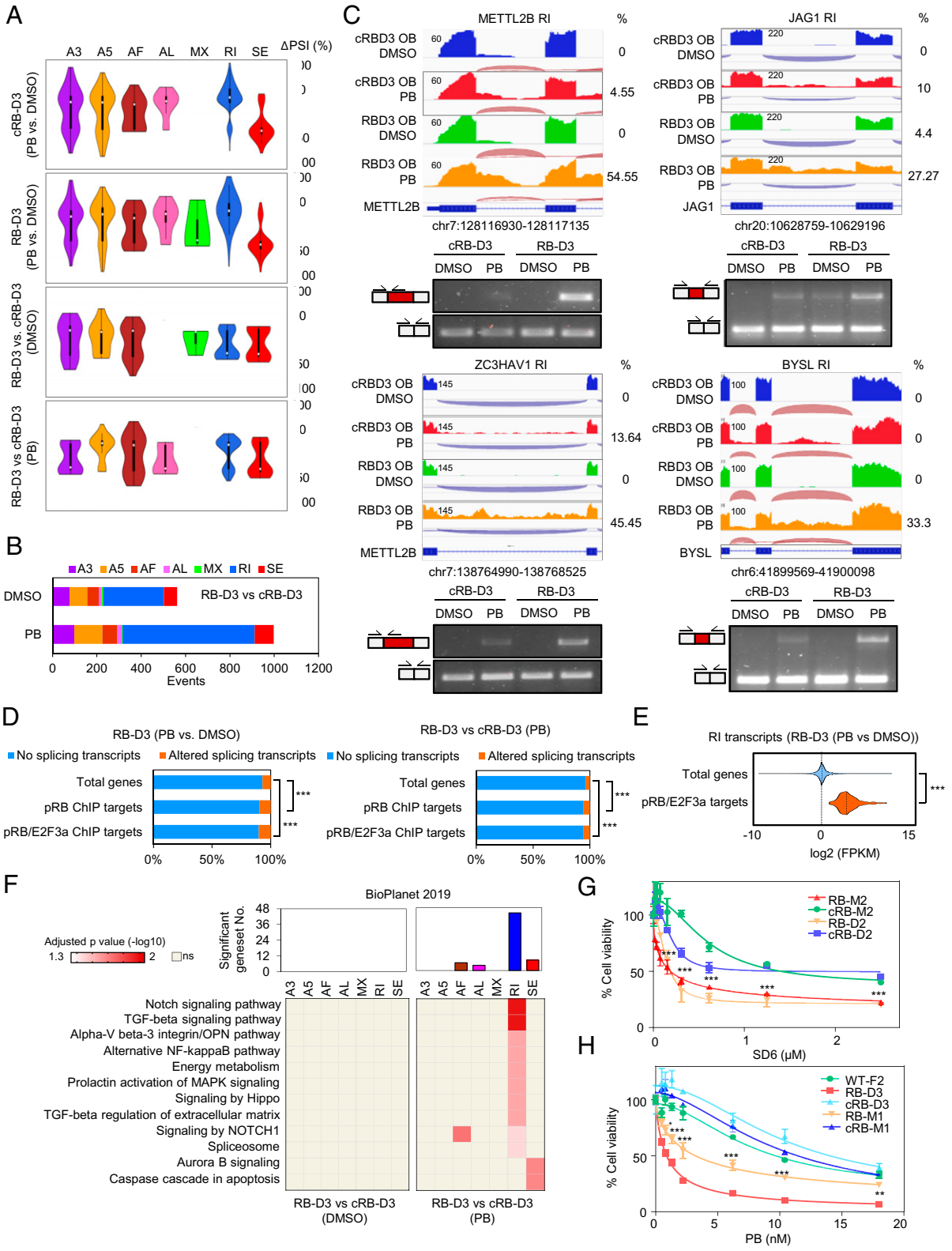

Fig. 4. Spliceosome perturbation influences cell viability and RNA splicing of RB OBs. (*A*) Violin plots represent distributions of statistically significant ΔPSI values ($P < 0.05$) for different classes of RNA splicing events: A3, A5, AF, AL, MX, RI, and SE. Separate violins are displayed for each pairwise comparison of DMSO- or PB-treated cells, and the percentage of events is presented. ΔPSI values are shown for 1) PB-treated cRB OBs compared with DMSO-treated cRB OBs; 2) PB-treated RB OBs compared with DMSO-treated RB OBs; 3) DMSO-treated RB OBs compared with DMSO-treated cRB OBs; and 4) PB-treated RB OBs compared with PB-treated cRB OBs. (*B*) Inhibition of spliceosomal function by PB leads to significant increases of aberrant RIs in RB OBs compared with cRB OBs. (*C*) Visualization of RNA-seq read mappings at *METTL2B*, *JAG1*, *ZC3HAV1*, and *BYSL* in the DMSO- and PB-treated OBs. A sashimi plot displaying the major splice junctions is superimposed. Representative RT-PCR validation of RI events of *METTL2B*, *JAG1*, *ZC3HAV1*, and *BYSL* transcripts. Exons are shown in gray and introns are in red. Half-arrows indicate the locations of primers designed to validate RI events. (*D*) Inhibition of spliceosomal function by PB preferentially alters RNA splicing events on pRB- and pRB/E2F3a–targeted transcripts. (*E*) *RB1* mutation–associated RI transcripts are more highly expressed than global transcripts in PB-treated RB OBs. FPKM, fragments per kilobase of exon per million mapped fragments. (*F*) Unique genes with perturbed splicing events in DMSO- or PB-treated cRB OBs vs. RB OBs are analyzed by BioPlanet 2019 and summarized by heatmaps. (*G* and *H*) Both PB and SD6 selectively inhibit the cell proliferation of RB OBs compared with cRB OBs. Results are expressed as mean ± SEM. **P* < 0.05, ***P* < 0.01, ****P* < 0.001.

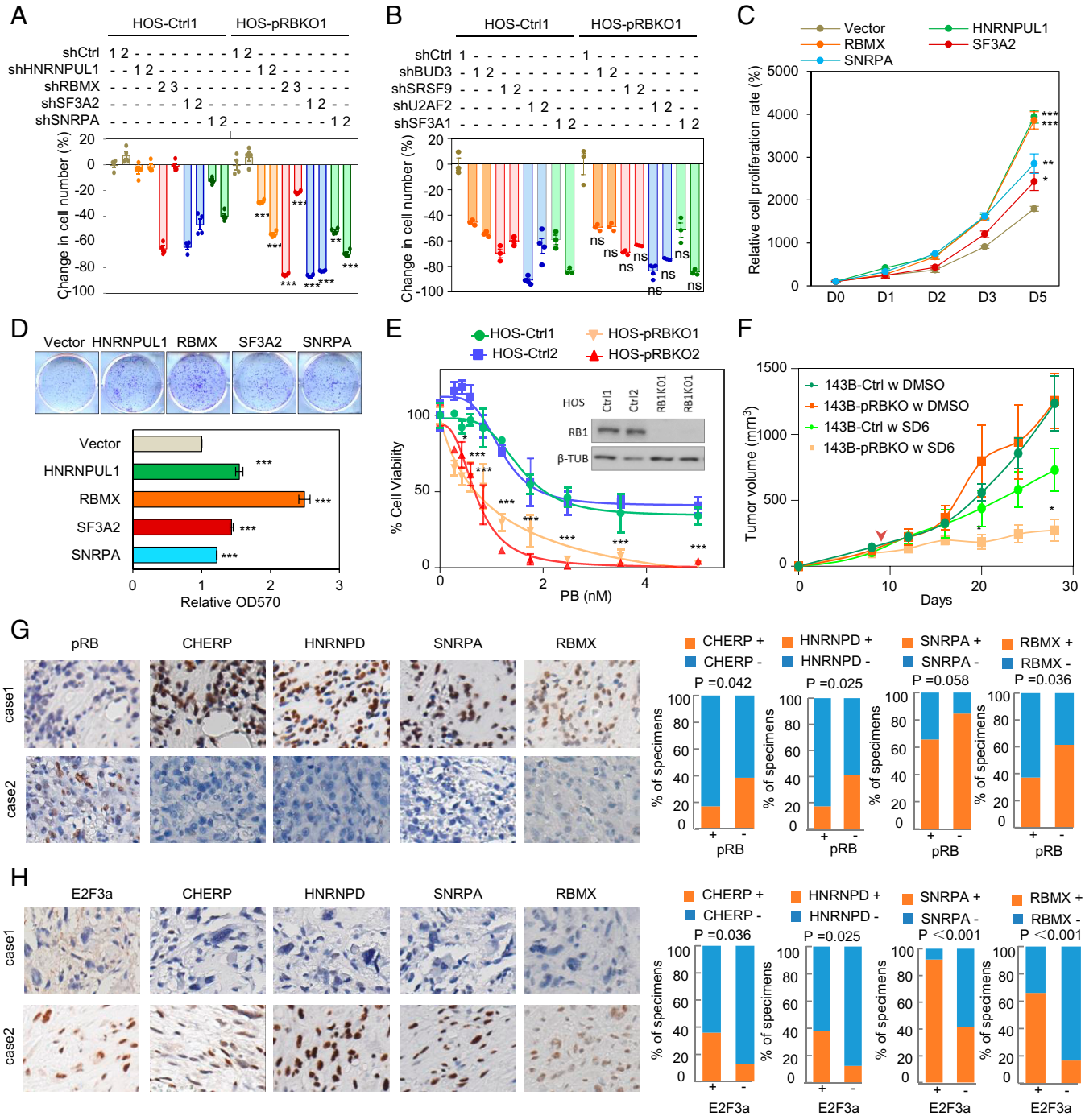

Fig. 5. OS specimens commonly have low pRB, high E2F3a, and high REOSS gene expression, and spliceosome inhibitors selectively impair pRB-deficient OS proliferation. (*A*) HOS-pRBKO cells are more sensitive to HNRNPUL1, RBMX, SF3A2, or SNRPA knockdown–induced inhibitory effects than HOS-Ctrl cells. (*B*) Knockdown of BUD31, SRSF9, U2AF2, or XAB2 showed similar inhibitory effects between HOS-Ctrl and HOS-pRBKO cells. (*C* and *D*) Ectopic expression of HNRNPUL1, RBMX, SF3A2, or SNRPA promotes HOS cell growth and colony formation. (*E*) PB selectively suppresses cell growth of HOS-pRBKO compared with HOS-Ctrl. (*F*) Spliceosome inhibitor SD6 preferentially suppresses pRB-deficient OS growth in vivo. Nude mice inoculated with 143B-Ctrl and 143B-pRBKO cells are injected with DMSO or SD6 (3 mg/kg) for four cycles (3-d constitutive injection and 1-d break) and the tumor growth is measured twice weekly. The arrowhead indicates the day of initial DMSO or SD6 injection. (*G*) pRB expression is negatively associated with CHERP, HNRNPD, SNRPA, and RBMX expression in 74 primary human OS specimens. (*G*, *Left*) Two representative specimens. (*G*, *Right*) Percentages of specimens with low (−) or high (+) pRB expression in which CHERP, HNRNPD, SNRPA, and RBMX are or are not observed. (*H*) E2F3a expression is positively correlated with CHERP, HNRNPD, SNRPA, and RBMX expression in 74 primary human OS specimens. (*H*, *Left*) Two representative specimens. (*H*, *Right*) Percentages of specimens with low (−) or high (+) E2F3a expression in which CHERP, HNRNPD, SNRPA, and RBMX are or are not observed. Results are expressed as mean ± SEM. ns, nonsignificant; $^{*}P < 0.05$, $^{**}P < 0.01$, $^{***}P < 0.001$.

rates of *RB1* gene mutation, including BLCA, BRCA, ESCA, HNSC, LIHC, LUAD, LUNG, LUSC, SARC, and OV (33). These pan-cancer transcriptional analyses using TCGA data further support the notion that the pRB/E2F3a–REOSS regulatory axis is a common pathway underlying cancer development.

Discussion

Recent studies have highlighted that several molecular subtypes of cancers are highly dependent on splicing function for cell survival and that pharmacological inhibition of the spliceosome

is a viable potential oncotherapeutic strategy (34–36). In contrast to most gene mutations, spliceosomal genes are frequently up-regulated in numerous cancers, suggesting that tumors rely on the spliceosome to produce cancer-associated splicing variants and overcome RNA transcriptional stress. The abundant up-regulation of spliceosomal genes observed in pRB-deficient cells likely represents tumor evolution to compensate for pRB loss–induced stress. The preferential lethality of RB OBs and pRB-deficient OS to pRB/E2F3a–regulated spliceosomal gene down-regulation and spliceosome inhibitors PB and SD6 compared with cells with intact pRB underscores the dependence of pRB-deficient tumors on spliceosome function. Our findings strongly suggest that spliceosome inhibitors should be considered in conjunction with current antineoplastic strategies to treat pRB-deficient associated malignancies.

Moreover, systemic chemotherapy and radiation therapy are independent risk factors for developing OS in RB patients (37). Chemotherapy and radiation treatments induce cancer cells to decrease the expression of spliceosomal genes, leading to intron retention in various genes (38). Inhibition of the spliceosome significantly impairs cellular response to DNA damage, which increases the selective lethality of cancer cells to chemotherapy. We suspect that the increase of spliceosomal genes in pRB-deficient cancers provides them with an indispensable advantage to repair chemo- and radiation-induced DNA damage, promote resistance to genotoxic stress, and survive following treatment.

Importantly, our findings show that pRB-deficient cells significantly lose growth and tumor formation potential upon REOSS gene knockdown or pharmacological inhibition of the spliceosome by either PB or SD6. pRB-deficient tumors appear exquisitely dependent on the spliceosomal machinery for growth and survival. In agreement with our findings, spliceosomal factors SRSF1 (39), PRPF6 (40), SRSF6 (41), and BUD31 (42) are either amplified or up-regulated in multiple cancers and function as oncoproteins by promoting tumorigenesis. Genetic or pharmacological inhibition of the spliceosome also selectively suppresses the proliferation and survival of cancers with elevated expression of these splicing factors, highlighting how inhibition of spliceosomal function is a general therapeutic strategy to treat cancers with dysregulated spliceosomal gene expression. Nonetheless, the full antitumor effects of spliceosome inhibitors on pRB-deficient cells may also involve genes not directly up-regulated by *RB1* inactivation. Together, we suggest that a large cohort of cancers driven by pRB deficiency, including OS, lung cancer, retinoblastoma, sarcoma, and breast cancers, are likely dependent on the spliceosome pathway for growth. pRB may also prove to be a useful biomarker for personalized therapeutics using spliceosome inhibitors.

Materials and Methods

Please see *SI Appendix, Materials and Methods* for a detailed description of materials and methods.

RNA-Seq. Time course samples of WT, RB, and cRB iPSC-derived MSCs and OBs were collected on days 0, 15, and 24. RB and cRB OBs were treated with 100 nM PB or dimethyl sulfoxide (DMSO) for 6 h. Cell samples were lysed in TRIzol reagent. RNA sample preparation and RNA-seq data analyses were performed as described previously (23).

ChIP-Seq and ChIP-qPCR. ChIP was performed using modified previous methods (5). For ChIP of pRB and 3×Flag-pRB, cells were prefixed for 30 min in 1.5 mM disuccinimidyl glutarate (Thermo Fisher Scientific, 20593) followed by fixation in 4% paraformaldehyde (Thermo Fisher Scientific, 28906) at room temperature for 10 min. For ChIP of E2F3a and 3×Flag-E2F3a, cells were cross-linked in 1% formaldehyde at room temperature for 10 min. After glycine quenching, cell pellets were collected and lysed and then subjected to sonication using a Branson Sonifier 450 (sonication conditions: 210 cycles, power 25%, 10 s on and 10 s off for pRB and 3×Flag-pRB; 150 cycles, power 25%, 10 s on and 10 s off for E2F3a and 3×Flag-E2F3a). The supernatant was then diluted in the same sonication buffer, and subjected to immunoprecipitation with corresponding antibodies at 4 °C overnight. The beads were then washed and DNA was reverse–cross-linked and purified. Following ChIP, DNA was quantified by qPCR using standard procedures. Sequencing libraries were prepared using the KAPA HyperPrep Kit (Roche, KK8502). The DNA was sequenced on an Illumina X10 platform using a PE150 Kit. ChIP-qPCR was performed using a CFX96 machine (Bio-Rad Laboratories). The 20-μL PCR solution was composed of 500 ng ChIP product, 1 μL, respectively, of 10 μM forward and reverse PCR primers for amplifying the peak region, 10 μL SYBR Green PCR Master Mix (Bio-Rad Laboratories, 1725124), and 7 μL RT-PCR–grade water. Primer sequences are listed in *SI Appendix*, Table S2.

Quantification and Statistical Analysis. All experiments were performed in at least biological triplicate, and all results are expressed as mean ± SEM. No statistical methods were used to predetermine sample size. Multiple *t* test, Student's *t* test, and one-way ANOVA followed by Student's *t* test (Tukey's multiple-comparison test) were applied to determine statistical significance in the experiments. Excel and GraphPad Prism 7.0 were used for the statistical analysis. ns, nonsignificant; $*P < 0.05$, $**P < 0.01$, $***P < 0.001$.

Data Availability. The RNA-seq, ChIP-seq, and WES data reported in this article have been deposited in the Gene Expression Omnibus repository under accession number GSE145235. Previously published data were used for this work (accession nos. GSE125903, GSE14827, and GSE36001). The data supporting the findings of this study are available within the article and *SI Appendix*.

ACKNOWLEDGMENTS. We thank Wenyi Wei for plasmids; Ying Liu, Yen-Ting Chiang, and D.-F.L. laboratory members for technical assistance and/or discussion; John F. Hancock and Kartik Venkatachalam for reagents and suggestions; and The University of Texas Health Science Center at Houston (UTHealth) Cancer Genomics Core for technical support and the next-generation sequencing service. We also acknowledge St. Jude Children's Research Hospital as the source of SD6. This work was mainly supported by UTHealth start-up funds (to D.-F.L., 37516-11998; to R.Z., 37516-11999), Cancer Prevention and Research Institute of Texas (CPRIT) RR16009 (to D.-F.L.), and NIH/NCI (National Cancer Institute) R01CA246130 (to D.-F.L., C.D.H., and R.Z.). This work was partially supported by a UTHealth Cancer Genomics Core Pilot Grant (to D.-F.L. and R.Z., CPRIT Grant RP180734). The UTHealth Cancer Genomics Core was supported by CPRIT RP180734. J.T. and Z.H. were supported by the Ke Lin Program Fellowship. J.T. was supported by the National Natural Science Foundation of China (Grant 82103078), and Z.H. was supported by the National Natural Science Foundation of China (Grant 82002510). A.X. was a CPRIT Postdoctoral Fellow in the Biomedical Informatics, Genomics and Translational Cancer Research Training Program (CPRIT Grant RP210045). D.Z. was supported by a Department of Defense Horizon Award (W81XWH-20-1-0389). Z.Z. was partially supported by the NIH/National Library of Medicine (R01LM012806) and CPRIT (RP180734 and RP210045). C.D.H. and Y.Y. were supported by the Andrew Sabin Family Foundation Fellowship. J. Shen was supported by the Scientific Research Cultivating Project of Sun Yat-sen University (Nos. 80000-18827202 and 80000-18823701), Fundamental Research Funds for the Central Universities (No. 19ykzd10), and Scientific Research 3 × 3 Project of Sun Yat-sen University (No. Y70215). D.-F.L. was supported by the CPRIT (RR160019), NIH/NCI R01CA246130, Rolanette and Berdon Lawrence Bone Disease Program of Texas, and a Pablove Foundation Childhood Cancer Research Grant (690785). D.-F.L. is a CPRIT Scholar in Cancer Research.

Author affiliations: [a]Department of Integrative Biology and Pharmacology, McGovern Medical School, The University of Texas Health Science Center at Houston, Houston, TX 77030; [b]Department of Musculoskeletal Oncology, The First Affiliated Hospital, Sun Yat-sen University, Guangzhou 510080, P. R. China; [c]Guangdong Provincial Key Laboratory of Orthopedics and Traumatology, The First Affiliated Hospital, Sun Yat-sen University, Guangzhou 510080, P. R. China; [d]Department of Endocrinology, The First Affiliated

Hospital, Sun Yat-sen University, Guangzhou 510080, P. R. China; [e]Department of Epidemiology, The University of Texas MD Anderson Cancer Center, Houston, TX 77030; [f]The University of Texas MD Anderson Cancer Center UTHealth Graduate School of Biomedical Sciences at Houston, Houston, TX 77030; [g]Center for Precision Health, School of Biomedical Informatics, The University of Texas Health Science Center at Houston, Houston, TX 77030; [h]Department of Biochemistry and Molecular Biology, McGovern Medical School, The University of Texas Health Science Center at Houston, Houston, TX 77030; [i]Department of Obstetrics & Gynecology and Women's Health, Einstein/Montefiore Medical Center, Bronx, NY 10461; [j]Center for Stem Cell and Regenerative Medicine, The Brown Foundation Institute of Molecular Medicine for the Prevention of Human Diseases, The University of Texas Health Science Center at Houston, Houston, TX 77030; [k]Wildflower Biopharma Inc., Encinitas, CA 92024; [l]Accutar Biotechnology Inc., Brooklyn, NY 11226; [m]Department of Neurology, Renaissance School of Medicine, Stony Brook University, Stony Brook, NY 11794; [n]Texas Children's Cancer and Hematology Centers, Baylor College of Medicine, Houston, TX 77030; [o]The Faris D. Virani Ewing Sarcoma Center, Baylor College of Medicine, Houston, TX 77030; [p]Department of Pediatrics, Texas Children's Hospital, Baylor College of Medicine, Houston, TX 77030; [q]Graduate Institute of Biomedical Sciences, China Medical University, Taichung 404, Taiwan; [r]Center for Molecular Medicine, China Medical University, Taichung 404, Taiwan; and [s]Department of Biotechnology, Asia University, Taichung 413, Taiwan

Author contributions: J.T., Z.H., Y.Y., A.X., N.R.F.-C., S.X.L.H., D.A.B., J.T.Y., L.L.W., M.-C.H., Z.Z., C.D.H., R.Z., and D.-F.L. designed research; J.T., Z.H., Y.Y., D.Z., A.X., M.-F.H., Y.-H.C., R.Z., and D.-F.L. performed research; T.R.W., M.-C.H., and J. Shen contributed new reagents/analytic tools; J.T., Z.H., Y.Y., D.Z., A.X., M.-C.H., R.H., R.W., J.A.G., K.-L.T., S.X.L.H., J. Su, P.J., Z.Z., C.D.H., R.Z., and D.-F.L. analyzed data; and J.T., J.A.G., D.A.B., R.Z., and D.-F.L. wrote the paper.

1. X. Graña, J. Garriga, X. Mayol, Role of the retinoblastoma protein family, pRB, p107 and p130 in the negative control of cell growth. *Oncogene* **17**, 3365–3383 (1998).
2. E. S. Knudsen, K. E. Knudsen, Tailoring to RB: Tumour suppressor status and therapeutic response. *Nat. Rev. Cancer* **8**, 714–724 (2008).
3. F. L. Wong *et al.*, Cancer incidence after retinoblastoma. Radiation dose and sarcoma risk. *JAMA* **278**, 1262–1267 (1997).
4. Y. H. Lin *et al.*, Osteosarcoma: Molecular pathogenesis and iPSC modeling. *Trends Mol. Med.* **23**, 737–755 (2017).
5. A. Chicas *et al.*, Dissecting the unique role of the retinoblastoma tumor suppressor during cellular senescence. *Cancer Cell* **17**, 376–387 (2010).
6. K. I. Hilgendorf *et al.*, The retinoblastoma protein induces apoptosis directly at the mitochondria. *Genes Dev.* **27**, 1003–1015 (2013).
7. C. H. Coschi *et al.*, Haploinsufficiency of an RB-E2F1-Condensin II complex leads to aberrant replication and aneuploidy. *Cancer Discov.* **4**, 840–853 (2014).
8. A. L. Manning *et al.*, Suppression of genome instability in pRB-deficient cells by enhancement of chromosome cohesion. *Mol. Cell* **53**, 993–1004 (2014).
9. A. L. Manning, M. S. Longworth, N. J. Dyson, Loss of pRB causes centromere dysfunction and chromosomal instability. *Genes Dev.* **24**, 1364–1376 (2010).
10. R. Vélez-Cruz *et al.*, RB localizes to DNA double-strand breaks and promotes DNA end resection and homologous recombination through the recruitment of BRG1. *Genes Dev.* **30**, 2500–2512 (2016).
11. R. Cook *et al.*, Direct involvement of retinoblastoma family proteins in DNA repair by non-homologous end-joining. *Cell Rep.* **10**, 2006–2018 (2015).
12. M. García-Cao, S. Gonzalo, D. Dean, M. A. Blasco, A role for the Rb family of proteins in controlling telomere length. *Nat. Genet.* **32**, 415–419 (2002).
13. C. A. Ishak *et al.*, An RB-EZH2 complex mediates silencing of repetitive DNA sequences. *Mol. Cell* **64**, 1074–1087 (2016).
14. Y. Shi, Mechanistic insights into precursor messenger RNA splicing by the spliceosome. *Nat. Rev. Mol. Cell Biol.* **18**, 655–670 (2017).
15. A. Sveen, S. Kilpinen, A. Ruusulehto, R. A. Lothe, R. I. Skotheim, Aberrant RNA splicing in cancer; expression changes and driver mutations of splicing factor genes. *Oncogene* **35**, 2413–2427 (2016).
16. E. El Marabti, I. Younis, The cancer spliceome: Reprograming of alternative splicing in cancer. *Front. Mol. Biosci.* **5**, 80 (2018).
17. V. I. Rasheva, D. Knight, P. Bozko, K. Marsh, M. V. Frolov, Specific role of the SR protein splicing factor B52 in cell cycle control in *Drosophila*. *Mol. Cell. Biol.* **26**, 3468–3477 (2006).
18. J. Ceron *et al.*, Large-scale RNAi screens identify novel genes that interact with the *C. elegans* retinoblastoma pathway as well as splicing-related components with synMuv B activity. *BMC Dev. Biol.* **7**, 30 (2007).
19. M. G. Oser *et al.*, Cells lacking the *RB1* tumor suppressor gene are hyperdependent on Aurora B kinase for survival. *Cancer Discov.* **9**, 230–247 (2019).
20. R. Brough *et al.*, Identification of highly penetrant Rb-related synthetic lethal interactions in triple negative breast cancer. *Oncogene* **37**, 5701–5718 (2018).
21. J. Ahlander, G. Bosco, The RB/E2F pathway and regulation of RNA processing. *Biochem. Biophys. Res. Commun.* **384**, 280–283 (2009).
22. X. H. Zhang, L. Y. Tee, X. G. Wang, Q. S. Huang, S. H. Yang, Off-target effects in CRISPR/Cas9-mediated genome engineering. *Mol. Ther. Nucleic Acids* **4**, e264 (2015).
23. D. F. Lee *et al.*, Modeling familial cancer with induced pluripotent stem cells. *Cell* **161**, 240–254 (2015).
24. R. Zhou *et al.*, Modeling osteosarcoma using Li-Fraumeni syndrome patient-derived induced pluripotent stem cells. *J. Vis. Exp.* (136), 57664 (2018).
25. H. Kim *et al.*, Oncogenic role of SFRP2 in p53-mutant osteosarcoma development via autocrine and paracrine mechanism. *Proc. Natl. Acad. Sci. U.S.A.* **115**, E11128–E11137 (2018).
26. D. M. Thomas *et al.*, The retinoblastoma protein acts as a transcriptional coactivator required for osteogenic differentiation. *Mol. Cell* **8**, 303–316 (2001).
27. J. R. Batanian *et al.*, Evaluation of paediatric osteosarcomas by classic cytogenetic and CGH analyses. *Mol. Pathol.* **55**, 389–393 (2002).
28. X. Chen *et al.*; St. Jude Children's Research Hospital–Washington University Pediatric Cancer Genome Project, Recurrent somatic structural variations contribute to tumorigenesis in pediatric osteosarcoma. *Cell Rep.* **7**, 104–112 (2014).
29. L. A. Gilbert *et al.*, CRISPR-mediated modular RNA-guided regulation of transcription in eukaryotes. *Cell* **154**, 442–451 (2013).
30. N. A. Kearns *et al.*, Cas9 effector-mediated regulation of transcription and differentiation in human pluripotent stem cells. *Development* **141**, 219–223 (2014).
31. D. R. Okoro, M. Rosso, J. Bargonetti, Splicing up mdm2 for cancer proteome diversity. *Genes Cancer* **3**, 311–319 (2012).
32. C. Lagisetti *et al.*, Optimization of antitumor modulators of pre-mRNA splicing. *J. Med. Chem.* **56**, 10033–10044 (2013).
33. P. Jia, Z. Zhao, Characterization of tumor-suppressor gene inactivation events in 33 cancer types. *Cell Rep.* **26**, 496–506.e3 (2019).
34. S. C. Lee, O. Abdel-Wahab, Therapeutic targeting of splicing in cancer. *Nat. Med.* **22**, 976–986 (2016).
35. S. Bonnal, L. Vigevani, J. Valcárcel, The spliceosome as a target of novel antitumour drugs. *Nat. Rev. Drug Discov.* **11**, 847–859 (2012).
36. D. P. Steensma *et al.*, Phase I first-in-human dose escalation study of the oral SF3B1 modulator H3B-8800 in myeloid neoplasms. *Leukemia* **35**, 3542–3550 (2021).
37. P. Temming *et al.*, Incidence of second cancers after radiotherapy and systemic chemotherapy in heritable retinoblastoma survivors: A report from the German reference center. *Pediatr. Blood Cancer* **64**, 71–80 (2017).
38. K. S. Anufrieva *et al.*, Therapy-induced stress response is associated with downregulation of pre-mRNA splicing in cancer cells. *Genome Med.* **10**, 49 (2018).
39. R. Karni *et al.*, The gene encoding the splicing factor SF2/ASF is a proto-oncogene. *Nat. Struct. Mol. Biol.* **14**, 185–193 (2007).
40. A. S. Adler *et al.*, An integrative analysis of colon cancer identifies an essential function for PRPF6 in tumor growth. *Genes Dev.* **28**, 1068–1084 (2014).
41. M. Cohen-Eliav *et al.*, The splicing factor SRSF6 is amplified and is an oncoprotein in lung and colon cancers. *J. Pathol.* **229**, 630–639 (2013).
42. T. Y. Hsu *et al.*, The spliceosome is a therapeutic vulnerability in MYC-driven cancer. *Nature* **525**, 384–388 (2015).